applied sciences

MDPI

Article

Influence of Hard Segments on the Thermal, Phase-Separated Morphology, Mechanical, and Biological Properties of Polycarbonate Urethanes

Rong Zhu [1,2], Xinyu Wang [1,2,*], Jing Yang [3], Yiyu Wang [1,2], Zongrui Zhang [1,2], Yuanjing Hou [1,2], Fei Lin [1,2] and Yi Li [4]

1 State Key Laboratory of Advanced Technology for Materials Synthesis and Processing, Wuhan University of Technology, Wuhan 430070, China; whutzhurong@gmail.com (R.Z.); yiyiyuyu.7@163.com (Y.W.); ruibeatthem@gmail.com (Z.Z.); houyuanjing–714@163.com (Y.H.); linfei@whut.edu.cn (F.L.)
2 Biomedical Materials and Engineering Research Center of Hubei Province, Wuhan University of Technology, Wuhan 430070, China
3 School of Foreign Languages, Wuhan University of Technology, Wuhan 430070, China; yjwhut@hotmail.com
4 Institute of Textiles and Clothing, The Hong Kong Polytechnic University, Hung Hom, Kowloon, Hong Kong, China; tcliyi@polyu.edu.hk
* Correspondence: wangxinyu@whut.edu.cn; Tel.: +86-27-8765-1853; Fax: +86-27-8788-0734

Academic Editors: Daniel X. B. Chen and Hidenori Otsuka
Received: 9 December 2016; Accepted: 16 March 2017; Published: 20 March 2017

Abstract: In this study, we have fabricated a series of polycarbonate polyurethanes using a two-step bulk reaction by the melting pre-polymer solution-casting method in order to synthesize biomedical polyurethane elastomers with good mechanical behavior and biostability. The polyurethanes were prepared using dibutyltin dilaurate as the catalyst, poly(1,6-hexanediol)carbonate microdiols (PCDL) as the soft segment, and the chain extender 1,4-butanediol (BDO) and aliphatic 1,6-hexamethylene diisocyanate (HDI) as the hard segments. The chemical structures and physical properties of the obtained films were characterized by attenuated total reflectance Fourier transform infrared (ATR-FTIR) spectroscopy, gel permeation chromatography (GPC), differential scanning calorimeter (DSC), and mechanical property tests. The surface properties and degrees of microphase separation were further analyzed by water droplet contact angle measurements (CA) and atomic force microscopy (AFM). The materials exhibited a moderate toxic effect on the tetrazolium (MTT) assay and good hemocompatibility through hemolytic tests, indicating a good biocompatibility of the fabricated membranes. The materials could be considered as potential and beneficial suitable materials for tissue engineering, especially in the fields of artificial blood-contacting implants or other biomedical applications.

Keywords: polyurethanes; hard segment; mechanical behavior; biocompatibility

1. Introduction

Biomedical polyurethane devices, because of their excellent mechanical flexibility, chemical resistance, and good biocompatibility [1–4], have been deeply investigated and widely used in the medical fields of both engineering and countless biomedical consumer products such as artificial hearts, catheters, injectable gels, pacemaker leads, and biodegradable scaffolds [5–9]. Most polyurethanes are multiblock co-polymers commonly consisting of hard and soft segments. For these types of materials, the various thermal and mechanical properties are determined by these alternating segments, repeating units of urethane linkages made by the reaction of an isocyanate with hydroxyl in polyurethanes, and especially the strong intermolecular forces of the hard domains [10,11]. In order to cater to specific property requirements, a large number of different polyurethanes were synthesized from the

reaction between diisocyanate, microdiols, and the chain extender [12–14]. The elastic deformability of elastomers is of great importance for all kinds of polyurethanes. Their available properties are directly related to the two phase microphase separation morphology caused by their unique structure of alternating hard and soft segments [15]. Investigators have devoted themselves to this field for at least fifty years, and have made great strides in understanding their excellent properties, attributed to their synthetic methods and chemical structures [16,17].

The mechanical properties are influenced by the type of diisocyanate, microdiols, the chain extender, and especially the urethane linkages of the hard segments [18–21]. The material will be broken when the local strength is more than the limited strength giving rise to the rupture of the local molecular chains. For the hard segment, the polyfunctional isocyanate can be divided into aliphatic, aromatic, polycyclic, or cycloaliphatic. 1,6-hexamethylene diisocyanate (HDI) is a kind of aliphatic diisocyanate, replacing aromatic ones which may release toxic components like 4,4′-methylenediphenyl diisocyanate (MDI) and toluene diisocyanates (TDI) after degradation [22–24]. For many medical devices, where excellent histocompatibility and blood compatibility of the materials are seriously required, the widely used poly(1,6-hexanediol)carbonate microdiol (PCDL) based polyurethanes exhibit excellent biostable elastic properties after exposure to oxidative, hydrolytic, and other biological solutions [25–27]. However, little attention has been paid to the comprehensive investigation of the relationship between the content of the hard segment and mechanical properties, particularly the phase-separated microstructure, crystallization behavior, surface performance, and biocompatibility.

In this work, biomedical polyurethane materials with various contents of the hard segment were synthesized through the melting pre-polymer method using PCDL (Mw = 2000 Da) as soft segments, and using 1,6-hexamethylene diisocyanate (HDI) and 1,4-butanediol (BDO) as the hard segments. In the present study, the physical and chemical properties of the polyurethanes were studied by FTIR, differential scanning calorimeter (DSC), gel permeation chromatography (GPC), and mechanical tests, and the maximum tensile elongation was about 500%. We have concluded that with the increment of different contents of the hard segment (less than 35%), the degree of microphase separation increased while the mechanical behavior of the prepared poly(carbonate-urethane) elastomers slightly decreased. Finally, hemolytic tests and the MTT assay were carried out using adult rabbit blood and L929 fibroblast cells to assess hemocompatibility and cellular viability in vitro, indicating a good biocompatibility of the fabricated membranes.

2. Experimental Methods

2.1. Materials

N,*N*-dimethyl acetamide (DMAc), tetrahydrofuran (THF), dibutyltin dilaurate, and diethyl ether were all purchased from Sinopharm Chemical Reagent Co., Ltd. (Beijing, China). PCDL (Mn = 2000 g·mol^{-1}) was obtained from Hersbit Chemical Co. Ltd. (Shanghai, China) and was stored at ordinary temperatures after drying at about 110 °C for 24 h in vacuum before use. Aliphatic 1,6-hexamethylene diisocyanate (99%) was purchased from TCI (Tokyo, Japan) and was stored at almost 0 °C in the refrigerator to prevent water molecules from entering the compound. Dibutyltin dilaurate (DBTDL) was added at a concentration of about 0.1 mass % while 1,4-butanediol (BDO) were dried over molecular sieves (0.4 nm) at room temperature overnight. The commonly used catalyst and chain extender in the biomedical polyurethanes synthesis procedure were used without further purification. The structure of all reactants used in this study are clearly illustrated in Figure 1.

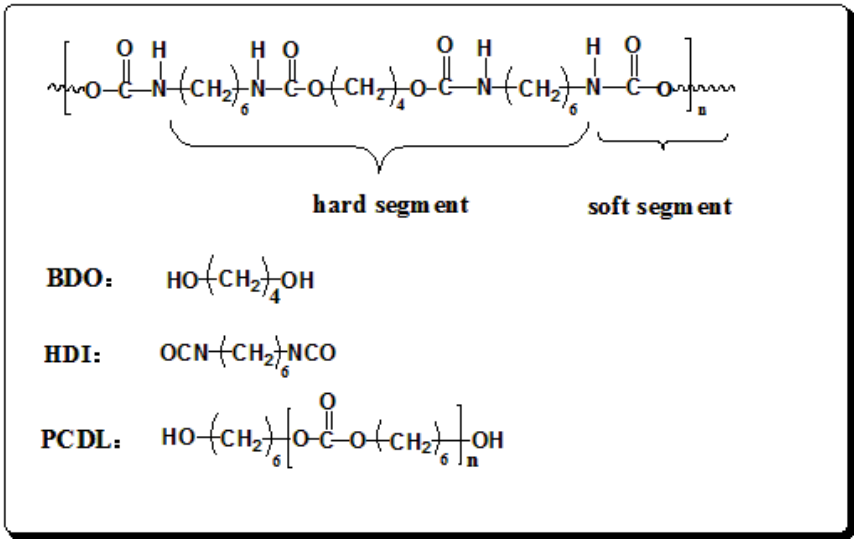

Figure 1. The chemical structures of the components in the polyurethanes.

2.2. Synthesis and Preparation of Polyurethane Films

The polyurethane elastomers were prepared through the melting pre-polymer method with a constant isocyanate index (the molar ratio of isocyanate groups to hydroxyl groups, NCO/OH = 1.05:1) [28]. In order to perform the experiment well, the materials for the experiment should be fully dried and the experiment should be carried out under nitrogen protection to limit water vapor. Only after dissolving in *N*,*N*-dimethylacetamide (30 wt %) could the reagents be added to the reaction flask. The polyurethane films can be easily prepared by a two-step reaction using PCDL and HDI with the chain extender BDO and dibutyltin dilaurate as the catalyst.

Firstly, the PCDL was added in a 250 mL dry four-neck round-bottom flask equipped with a depressurizing system, a heating mantle with a small magnet for stirring, and reflux condenser at about 110 °C for several hours until there were no bubbles, to eliminate water molecules from entering the reaction. After cooling down to about 40 °C and equipping the nitrogen gas inlet system in exchange for the depressurizing system, different proportions of HDI and DBTDL were added to the reaction mixture in a dropwise manner. Then, after the reaction proceeded for four hours, the remaining HDI as well as BDO were added to the prepared solution according to the requirements with a high stirring rate of 800 r/min at 40–45 °C for at least 10 h. After that, the mixed solution was put into a beaker for precipitation with ether-water with a proportion of 3/7 (v/v). Then the polymer was placed in a simple Soxhlet extractor using ultrapure water as the extracting agent to remove unreacted monomers and small molecules such as ether for at least 20 h. After drying in a vacuum drying chamber, the polymers were dissolved in tetrahydrofuran and placed in a vacuum oven at 45 °C to 50 °C with a mass concentration of 8%.

2.3. Characterization Methods

The FTIR spectra were obtained by VERTEX80v Fourier transform infrared spectroscopy (Bruker, Karlsruhe, Germany). All spectra were recorded between 4000 cm^{-1} and 400 cm^{-1} with 64 scans and a resolution of 4 cm^{-1}. The data were prepared to fit the combination of a Lorentzian and Gaussian curve by Origin-Pro 8.5 (OriginLab, Northampton, MA, USA, 2012).

Thermal behaviors were analyzed with a Diamond DSC (PerkinElmer, Waltham, MA, USA), such as the melting and transition temperatures, and crystallization behavior of the PCUs. Liquid N_2 was used to cool the DSC cell to obtain sub-ambient temperatures. All the samples were sealed in aluminum pans with sample weights ranging from 9 to 15 mg. The experiment was carried out under a constant nitrogen flow at a heating rate of 5 °C/min. After eliminating the thermal history,

the melting point and the glass transition temperature were taken from the second heating curve after a 2 min station behind the first heating.

The mechanical behavior of the films was determined at room temperature after two weeks by a mechanical testing machine, a computer controlled hydraulic universal testing machine (M-30A, Shenzhen, China), using a crosshead speed of 50 mm·min^{-1}. The tensile tests of the films were based on ASTM D882-12. At least six specimen determinations were conducted for each type of film to obtain the average value.

The relative molecular mass of the pre-polymers and their distribution were determined by gel permeation chromatography (GPC) measurements, using an Alliance high performance liquid chromatography analyzer (Waters, Milford, MA, USA). Tetrahydrofuran was employed as the eluent at a flow rate of 1.000 mL/min at 30 °C. According to ASTM D6579-6, in order to determine the retention time data, number, and molecular weights, we calibrated the whole system with the monodisperse polystyrene distribution curve ranging from 2.98 to 706 kg/mol as the general calibration parameter.

The phase-separated morphology observations were conducted on a flat mica substrate. Measurements were performed under ordinary conditions using a commercial atomic force microscope (Multimode 8 AFM, Bruker, Madison, WI, USA) equipped with Silicon TESP cantilevers in a non-contact (tapping) mode (Nanosensors PPP-NCH, spring constant 10–130 N). The data of the surface images were analyzed with NanoScope Analysis software (Bruker, Madison, WI, USA).

The goniometer (OCA-35, Dataphysics, Stuttgart, Germany) was employed to measure the static contact angles of water droplets with the samples. Firstly, a piece of silicon wafer (nearly 1 × 1 cm^2) with the attached membrane was placed on the goniometer. Then, the liquid (ultrapure water, less than 1 μL in volume) was dropped for testing. At least 3 measurements were taken for each surface on the air-exposed side at different locations. Finally, the average value was calculated using the in-built software.

Animal experiments were approved by the Review Committee for the Use of Human or Animal Subjects of Wuhan University of Technology and conducted in accordance with the Declaration of Helsinki and with the Guide for Care and Use of Laboratory Animals as adopted and promulgated by the United National Institutes of Health. The normal L929 fibroblast cells and adult rabbit blood were used for the MTT assay and hemolytic tests, evaluating the cytotoxicity of the fabricated membranes through cellular viability and hemocompatibility tests. The experiments were carried out as previously reported [29,30]. The cell morphology in different leaching liquor was observed through an Inversion fluorescence microscope (Olympus IX71, Tokyo, Japan), while cell viability was evaluated by a universal microplate spectrophotometer (Thermo Labsystems 1500-206, Waltham, MA, USA) with a 550 nm filter.

3. Results and Discussion

3.1. Molecular Weight Determination

Table 1 showed the molecular mass of the polyurethane samples with different weights of the hard segment, indicating that the weight average molecular weight and number average molecular weight increased with increasing weight of the hard segment. The range of the number-average molecular weight was 0.88 × 10^4–2.66 × 10^4 Da with the molecular weight distributions between 1.20 and 1.68, indicating that the molecular weight becomes better with a better distribution with increasing the hard segment. This result can be attributed to many factors, such as water molecules present in the raw material of HDI forming amine groups and the degree of microphase separation increasing with the increase of the hard segment. As we know, there are certain relations between the molecular weight and mechanical properties. Generally speaking, a relatively larger molecular weight will reveal better physical performance, having a great influence on applications in the biomedical materials field [31].

Table 1. Molecular weights and molecular weight distributions of the synthesized polycarbonate urethanes (PCUs) used in this work. Here, polyurethanes are denoted as PCU-x%, where x is the hard segment weight fraction.

Samples	$Mn \times 10^4$(Da)	$Mw \times 10^4$(Da)	PDI (Mw/Mn)
PCU-20%	2.66	4.47	1.68
PCU-25%	1.37	2.08	1.52
PCU-30%	0.92	1.14	1.23
PCU-35%	0.88	1.06	1.20

3.2. ATR-FTIR Analysis

The FTIR spectra of the raw material and the obtained prepared films are illustrated in Figure 1. It was obvious that the spectra of the typical signals of the prepared films were similar. It was reasonable that the main hard segment content and groups of the polyurethanes were almost the same. The main absorption bands were as follows: 3320 cm^{-1} (N–H stretching); 2870 cm^{-1} (CH_2 stretching) (polycarbonate diol); 2939 cm^{-1} (CH_2 asymmetrical stretching) (polycarbonate diol); 790 cm^{-1} (C–O–C asymmetrical stretching); and 1242 cm^{-1} (O=C–O asymmetric bending). The following bands prove that the structure of the polycarbonate polyurethane polymer was successfully synthesized. The 1731 cm^{-1} band of the polyurethane film was broader than PCDL where splitting into 1737 cm^{-1} and 1680 cm^{-1} bands occurred, and carbonyl stretching vibration of the carbamic acid ester at 1537 cm^{-1} (C–N–H in-plane bending). The presence of non-bonded groups could be attributed to the high structural symmetry of the chain extender, and could inhibit the ordering by existing in the hard domain formation. Additionally, none of the curves exhibited a typical absorption peak at about 2270 cm^{-1}, indicating that all of the –NCO groups were removed during the Soxhlet extraction.

Generally speaking, some hydrogen bonds are also involved in polyurethanes, taking the amide and the carbonyl groups as the donor and acceptor, respectively. Hydrogen–bonded N–H stretching vibrations in the urethane unit region is located at 3320 cm^{-1} for all the polyurethane samples as shown in Figure 2, where PCU-30% is higher than those for the other samples, showing the most strengthened hydrogen bonding within relatively better feed ratios of the hard segments. This result suggested that PCU-30% could exhibit the highest degree of microphase separation between the hard and soft segments [32]. Therefore, from the discussion of the FTIR data, we can easily obtain the conclusion that we have successfully prepared the polymer membranes as shown in Figure 1.

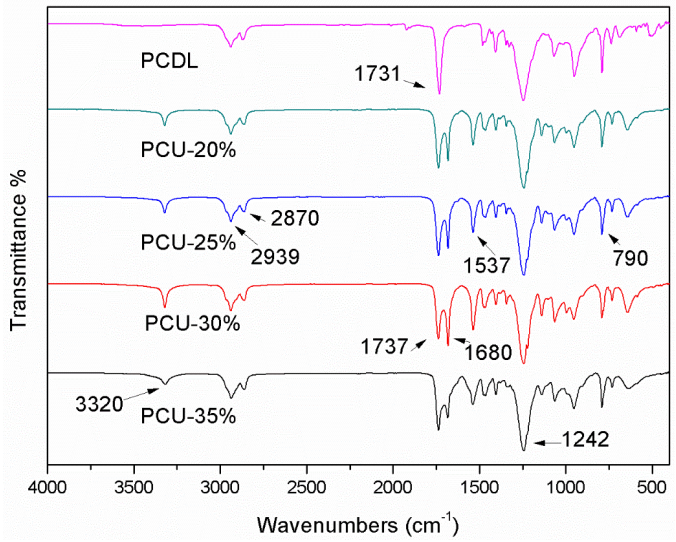

Figure 2. The FTIR spectra of poly(1,6-hexanediol)carbonate microdiols (PCDL) and the prepared polyurethane films.

3.3. The Surface Morphology and Wettability Analysis

The 3D perspectives of the surface topography of the prepared membranes were characterized by AFM at low tapping forces, indicating that the content of the hard segment in the PCUs had decisive influence on the surface morphology. As shown in Figure 3, the increment in the hard segment content had an obvious influence on the surface roughness of the films, resulting in a somewhat consequent decrease to make the processed surface much smoother. The mean roughness parameters ranged between 50 nm and 100 nm. By our knowledge of prior studies, a direct-viewing impression on the distribution of the microphase morphology could also be presented by the AFM images, not showing a clear phase contrast but merely indicating the hard domains appearing as extended lighter areas while the smaller darker areas represent the soft domains in the phase images [33]. The analysis of the AFM images in the probed regions clearly demonstrated that the microphase separation structures existed and that as the fraction of the hard segment composition increases, there were more hard segments involving in the lighter regions, exhibiting a greater degree of the discernible microphase separation with the average size of the hard domains between 5 and 10 nm. This result was also in agreement with the mechanical behavior of polyurethanes.

The wettability of the polyurethane membranes was determined by the static contact angle measurement at room temperatures and pressures (101 kpa). As mentioned in the initial literature and as promoted by Cassie-Baxter's law, the static contact angle on a specific solid/liquid surface greatly depended on the fraction of the trait of the solid [34]. Generally speaking, the relatively smaller contact angle (<90°) indicated a higher hydrophilic property of the surface while the relative larger contact angle (>90°) indicated a more hydrophobic property [35]. Figure 4 shows the static contact angles of polyurethane films with different contents of hard segments of the polyurethanes. It is noticeable that the contact angle increases gradually with increasing contents of the hard segment, which was also consistent with the analysis of the AFM images regarding the surface relief. As we know, the contact angle is related to the surface structure of the film and is controlled by fluid dynamics. Also, from the comparison of Table 1 and Figure 4, we can see that the angles changed with the molecular weight where the value of the contact angles increased with decreasing molecular weight, indicating the rising surface hydrophobic property. It has been proven that the surface roughness of the membrane surface has an inseparable relationship with the adhesion of protein in blood vessels, and affects the final applications of biomedical materials, especially for blood-compatible materials, indicating that with larger surface roughness, the lower the probability is to form blood clots [36]. When the contact angle increases, it goes against the adhesion procedure, making medical operations relatively easier to carry out. Additionally, for smaller molecular weights of polyurethane, the existence of more side chains may be another vital impact that leads to much better hydrophilicity with strong hydrogen bonding interactions. Biomaterials with high surface free energy would have a relative small contact angle value indicating good wettability. Additionally, the decrease of work adhesion could restrict the capability of the polyurethane surface to generate less hydrogen bonds with water molecules. The work of adhesion values (W_a) were calculated based on the following equation [37]:

$$W_a = \gamma\,(1 + \cos\theta) \tag{1}$$

where γ and θ represent the constants for surface tension of the fluid (water = 72.81 mN/m) and the static contact angle, respectively.

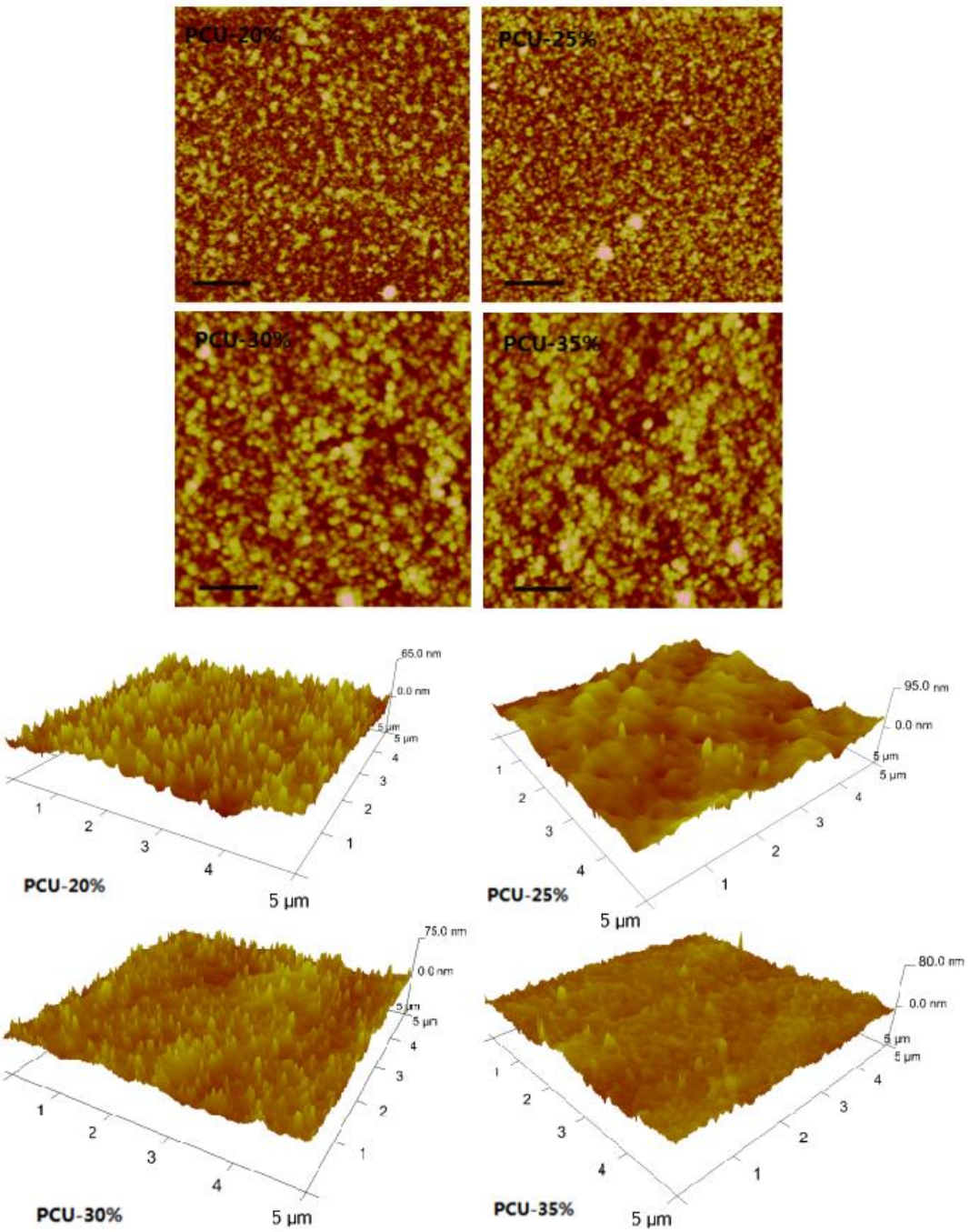

Figure 3. Atomic force microscopy images of surface relief (5 × 5 µm) and phase images (500 × 500 nm) of the films. The scan bar on the images is 100 nm.

From the analysis of the obtained data and calculated results, we can gain some insight towards enhancing the blood compatibility of organisms by modifications in the future. Based on these thoughts, we concentrated on other experiments associated with increasing the water contact angle to improve the biocompatibility of the materials.

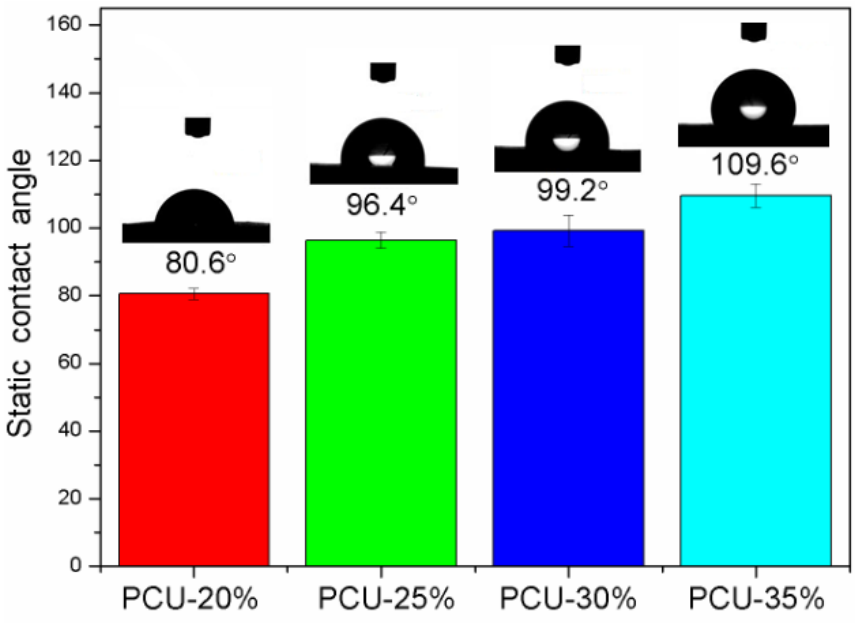

Sample	PCU-20%	PCU-25%	PCU-30%	PCU-35%
Contact angel (°)	80.6	96.4	9.2	109.6
Work of adhesion (mN/m)	84.70	56.58	61.17	48.39

Figure 4. Surface contact angles of the different contents of hard segments of the polyurethanes.

3.4. Differential Scanning Calorimetry

Figure 5 shows the DSC curve of the raw material PCDL and all types of PCUs. The left one was the DSC curve of PCDL with number 2 indicating the second heating process. The three melting peaks were quite obvious, which were the short-range order peak, long-range order peak, and micro crystal melting peak, respectively. The left one exhibited that the glass transition temperature of PCDL was approximately 40 °C, while the right one described the second heating process of the DSC curves of the polyurethane films based on different contents of the hard segment. There was an apparent distinction of the glass transition temperatures between the PCDL and the prepared polymer while the melting temperature of the polyurethanes stayed almost constant with little change at about 55 °C, attributed to the crystallization of the microphase separation. The relative percent crystallinity (R_c) of the PDCL in the PCUs was evaluated according to the enthalpy of fusion with the following equation:

$$R_c = \Delta H / (w_{ss} \times \Delta H^0) \times 100\% \quad (2)$$

where w_{ss} is the theoretical mass fraction of the soft segment, ΔH is the enthalpy of melting of the PCUs obtained experimentally, while ΔH^0 is the enthalpy of 100% crystalline PCDL (136 J·g^{-1}) [38].

Figure 5 shows the DSC curves of all types of PCUs; with the increment of the hard segment, the crystallization process was slightly enhanced, indicating that the polymers containing a relatively high content of hard segment were conductive to the crystallization process. Since we know that the hard segments have sufficient mobility when the temperature increases in the hard domains, to a certain extent, this phenomenon could be largely ascribed to the long HDI-BDO sequences. The results were also in agreement with the analysis of AFM and the mechanical properties.

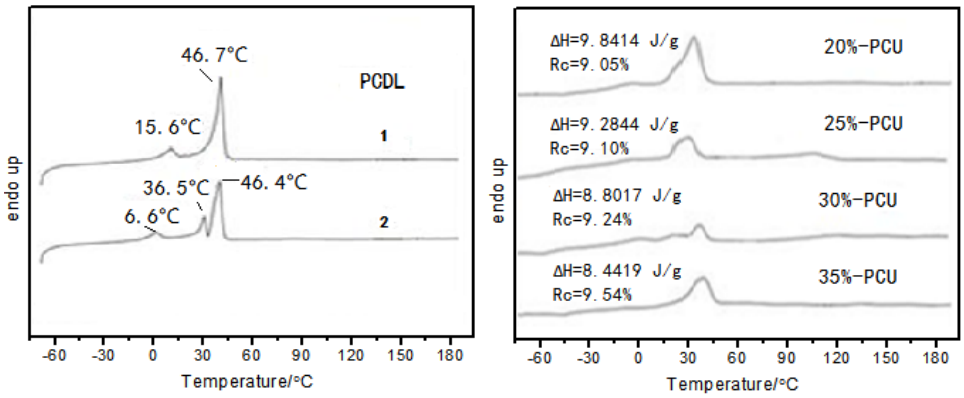

Figure 5. The DSC of the raw material PCDL and the prepared polymer.

3.5. Mechanical Properties Measurement

As we know, whether a material can be put into practical use greatly depends on its physical properties [39]. Figure 6 depicts the tensile stress-strain curves for the samples. The membranes with different contents of the hard segment of polyurethanes showed flexibility and typical nonlinear behaviors. The average values of the obtained numerical data about the tensile strength, elastic modulus, and other corresponding characteristic tensile parameters of the prepared films are given in Table 2. The PCUs showed tensile moduli in the range of 9.4–18.3 MPa and elongation at break in the range of 380%–530%. The mechanical behavior of the polyurethanes were dependent on several factors, such as the degree of crystallinity and microphase separation [40,41], concentration, and the interconnectivity of hard segments. Here, all samples containing hard segments with the same composition presented an amorphous structure, as already indicated by AFM. The increment in hard segment content brought about a consequent increase in the cross-linked density as well as the degree of ordering structures, and can also be an important factor related to the decreased values of the tensile modulus [42]. The 30%-PCU presented relatively lower ultimate tensile strength and greater elongation at break than the others. Moreover, it is worth noting that when the hard segment was 35%, the flexibility of the films decreased to a great extent. This may mainly result from the loss of the three-dimensional steric effect on the main chain of the macromolecules. Based on the analysis of the above-mentioned points, it was possible to conclude that the inter-molecular interaction provided by the increased crosslinking density (caused by the increased hard segment) tends to generate a secondary crystallization (soft segment) to limit the mobility of the chains, causing an increase in the values of the mechanical properties [43]. In each series, the material will be broken when the local strength is more than the limited strength, giving rise to the rupture of the local molecular chains, which was consistent with the theory [44]. As we know, the elongation is inversely proportional to brittleness. The analysis of the AFM images fully proved that the degree of the microphase separation enhanced with the increase of the hard segment. The deduction of deformability can be derived from the statistics in Table 2, which may be attributed to the increased hard segment phase gathered in the regions. The aggregation could result in a larger degree of microphase separation and a greater crystallization possibility of the soft segment, causing the material to become more brittle and the elongation at break to decrease. To some extent, the results indicated that the mechanical properties of the polymer were influenced by the proportion of the hard segment. In addition, there were other factors influencing the final physical performance, such as the possibility of a localization of shear stresses at the narrow interface occurring and the ratio of the hard/soft segment [45].

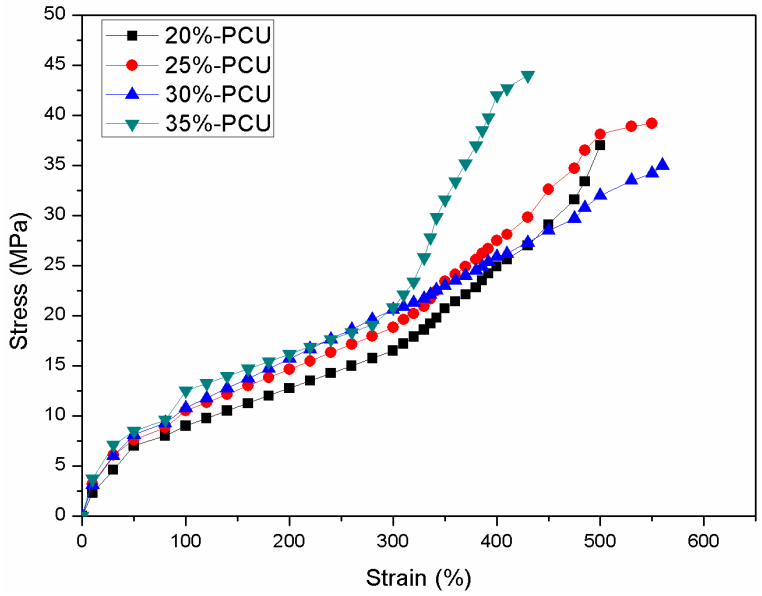

Figure 6. Tensile stress-strain curves of different contents of hard segments of the polyurethanes.

Table 2. Comparison between the polyurethane films and other commercial polyurethane products.

Samples	Tensile Modulus (MPa)	Ultimate Tensile Strength (MPa)	Elongation at Break (%)	Tensile Elongation (100%) Tensile Strength (MPa)	Tensile Elongation (300%) Tensile Strength (MPa)
20%-PCU	9.4 ± 1.4	35.6 ± 3.7	490 ± 50	8.7 ± 1.2	15.6 ± 2.1
25%-PCU	12.6 ± 1.1	38.5 ± 1.2	510 ± 70	10.2 ± 0.8	18.4 ± 1.6
30%-PCU	15.4 ± 3.1	30.5 ± 5.4	530 ± 30	10.3 ± 1.4	20.5 ± 1.2
35%-PCU	18.3 ± 2.7	43.3 ± 2.3	380 ± 50	11.6 ± 1.7	24.6 ± 1.5
Chronoflex® C	14.8 ± 1.8	45.5 ± 3.1	410 ± 30	-	-
Pellethane 2363-80A	13.0 ± 2.0	34.0 ± 2.0	430 ± 20	-	-

3.6. Hemolytic Experiments and Cytotoxicity Assay by MTT

Blood compatibility and cytotoxicity are extremely vital problems faced by biomaterial researchers, especially when considering implant biomaterials [46,47]. Red blood cells may rupture when they contact blood incompatible implant materials, releasing hemoglobin and blood platelets to form blood clots caused by their destruction [48]. In order to evaluate the hemolysis of the materials, all the data obtained from the hemolysis test were collected and calculated in Table 3. All of the films exhibited slightly hemolysis (under 3%), which conformed to the American Society for Testing and Materials standards, so as to be considered as blood compatible materials. The hemolysis ratio was evaluated according to the equation below:

$$HR(\%) = [(D_{sample} - D_{negative})/(D_{positive} - D_{negative})] \times 100\% \quad (3)$$

where HR represents the hemolysis ratio, and D_{sample}, $D_{negative}$, and $D_{positive}$ are the absorbance of the test samples, negative samples, and positive samples, respectively [49].

The hemolysis rates slightly decreased as the content of hard segment increased, which was in accordance with the analysis of the wettability of the membranes. Generally speaking, the lesser the HR value was, the better the blood compatibility of the material was. Therefore, the increment of the hard segment could lead to less damage of the red blood cells, showing desirable potential as a significant factor to obtain better blood compatibility for practical applications.

Table 3. Hematolysis ratio of all types of membranes.

Samples	Average Optical Density	Negative	Positive	Hemolysis Ratio (%)
20%-PCU	0.7175	0.0437	0.3642	2.1024
25%-PCU	0.6990	0.0437	0.3642	2.0446
30%-PCU	0.5339	0.0437	0.3642	1.5296
35%-PCU	0.5104	0.0437	0.3642	1.4560

The method of the MTT assay, for its simplicity and high reproducibility, is a widely performed strategy which is specifically used for mitochondrial function and to evaluate cytocompatibility of biomaterials for cell viability and proliferation [50]. The percentage viability of cell lines with 7 days of contact of primary L929 cells with the leaching liquor exposed to some representative PCUs films is shown in Figure 7. The percentage of viable cells with the obtained values were collected and calculated according to the following equation [51]:

$$\text{Cell viablitiy } (\%) = \frac{\text{Absorbance of samples and L929 cells} \times 100}{\text{Absorbance (control)}} \quad (4)$$

Generally speaking, cytotoxicity can be rated based on the above equation relative to the controls; severe cytotoxicity (<30%), moderate cytotoxicity (30%–60%), slight cytotoxicity (60%–90%), and not cytotoxic (>90%) [52]. Clearly, these membranes showed a cell viability response of over 70%, indicating that the produced polyurethanes could be classified into the level of slight cytotoxicity with relatively good biocompatibility. Obviously, all the groups with different contents of the hard segment exhibited significant differences and there were little changes in the cell viability with the increased hard segment. Furthermore, the PCU-30% group presented the relatively best results among them. As we know, a reason for the decrease of cell viability is that the hard segment of PCU can degrade and the degradation products may have a certain toxic effect on cells, reducing cell growth [53]. The morphology of L929 cells incubated with the leaching liquor after 3 days is also displayed in Figure 7. Thus, the analysis of our data gave clear evidence that the content of the hard segment of polyurethanes could slightly affect cell viability and consolidate cells.

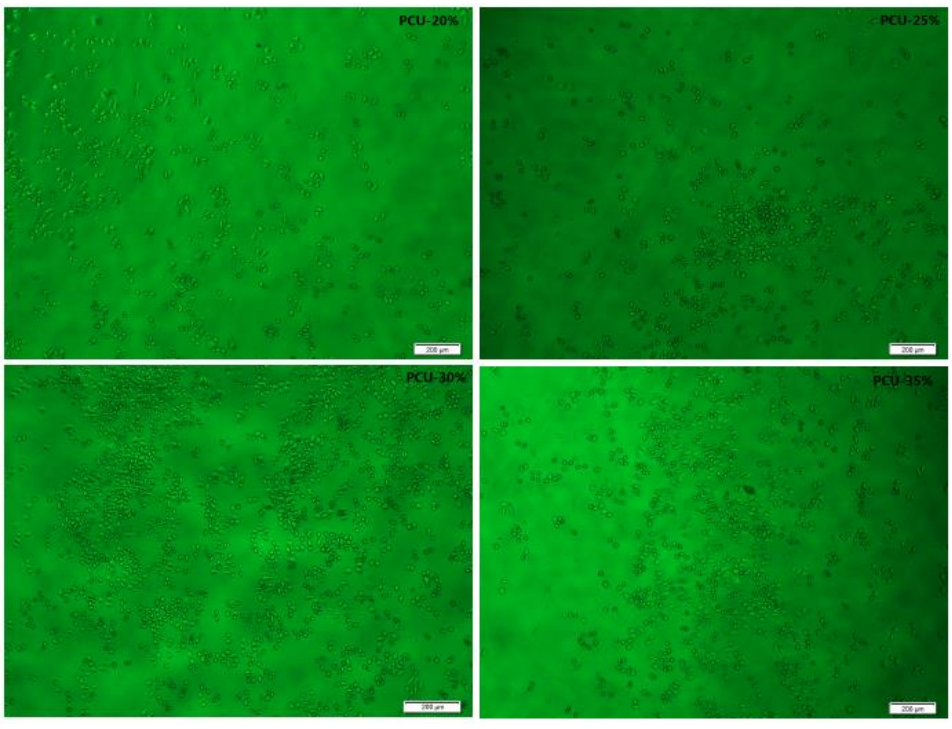

Figure 7. *Cont.*

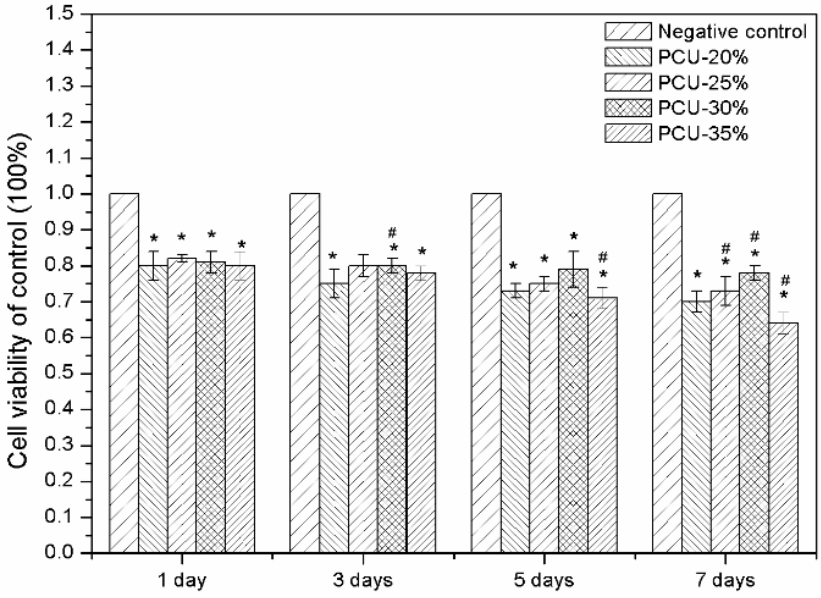

Figure 7. Micrographs of L929 cells with the materials and the toxicity of the membranes obtained by submersing the samples in media for 3 days. The scan bar on the images is 200 μm. A concentration series of high-density polyethylene liners served as the negative control ($n = 6$, $p < 0.05$, mean ± SD; *: represents a significant difference compared to the control. #: $p < 0.05$ significant below 70% value).

4. Conclusions

In this paper, different contents of the hard segment of polyurethanes were successfully synthesized using HDI, BDO, and PCDL via the melting polymerization method. The chemical structures of polymers were evaluated by the analysis of FT-IR images while the microphase separated structure crystallization behavior was characterized by AFM and DSC. The results and analysis showed that when we increased the content of the hard segments, the degree of the microphase structure and crystallization enhanced, while the surface of the membranes became more smooth, finally demonstrating that it could produce an effect on the physical behavior of the polyurethanes regarding the flexibility and elongation at break; they exhibit even better properties than other similar commercial polyurethanes while maintaining relatively high biocompatibility. This was especially true for PCU-30% as an elastic biomedical material, with a Young's modulus of 15.4 ± 3.1 MPa, tensile strength of 30.5 ± 5.4 MPa, and elongation at break of 530% ± 30%. Its biocompatibility was relatively the best among the materials, and it exhibits great potential for use in the fields of artificial blood-contacting implants or other biomedical engineering applications, by using extra procedures such as the use of surface treatments or co-polymerization to enhance histocompatibility and blood compatibility.

Meanwhile, we have made a stark comparison to other available commercial polyurethane products in the biomedical materials field, proving that the synthesized materials were found to be more flexible to meet the requirements of even higher mechanical properties, making them a certain potential prospect of tissue engineering applications in the biomaterials field in the future.

Acknowledgments: This work was supported by the Hong Kong, Macao, and Taiwan Science & Technology Cooperation Program of China (No. 2015DFH30180), the Key Technology Research Plan of Wuhan Municipality (No. 2014060202010120) and the Science and Technology Support Program of Hubei Province (No. 2015BCE022).

Author Contributions: Rong Zhu and Xinyu Wang conceived and designed the experiments; Rong Zhu and Yuanjing Hou performed the experiments; Yiyu Wang and Zongrui Zhang analyzed the data; Xinyu Wang and Fei Lin contributed reagents/materials/analysis tools; Rong Zhu, Jing Yang and Yi Li wrote the paper.

Conflicts of Interest: The authors declare no conflict of interest.

References

1. Heijkants, R.G.J.C.; van Calck, R.V.; van Tienen, T.G.; de Groot, J.H. Uncatalyzed synthesis, thermal and mechanical properties of polyurethanes based on poly (ε-caprolactone) and 1,4-butane diisocyanate with uniform hard segment. *J. Biomater.* **2005**, *26*, 4219–4228. [CrossRef] [PubMed]
2. Chattopadhyay, D.K.; Webster, D.C. Thermal stability and flame retardancy of polyurethanes. *J. Prog. Polym. Sci.* **2009**, *34*, 1068–1133. [CrossRef]
3. Madhavan, K.; Reddy, B.S.R. Synthesis and characterization of polyurethane hybrids: Influence of the polydimethylsiloxane linear chain and silsesquioxane cubic structure on the thermal and mechanical properties of polyurethane hybrids. *J. Appl. Polym. Sci.* **2009**, *113*, 4052–4065. [CrossRef]
4. Biemond, G.J.E.; Brasspenning, K.; Gaymans, R.J. Synthesis and selected properties of polyurethanes with monodisperse hard segments based on hexane diisocyanate and three types of chain extenders. *J. Appl. Polym. Sci.* **2012**, *124*, 1302–1315. [CrossRef]
5. Guelcher, S.A.; Srinivasan, A.; Dumas, J.E.; Didier, J.E. Synthesis, mechanical properties, biocompatibility, and biodegradation of polyurethane networks from lysine polyisocyanates. *J. Biomater.* **2008**, *29*, 1762–1775. [CrossRef] [PubMed]
6. Sarkar, S.D.; Farrugia, B.L.; Dargaville, T.R.; Dhara, S. Chitosan–collagen scaffolds with nano/microfibrous architecture for skin tissue engineering. *J. Biomed. Mater. Res. A* **2013**, *101*, 3482–3492. [CrossRef] [PubMed]
7. Parrag, I.C.; Woodhouse, K.A. Development of biodegradable polyurethane scaffolds using amino acid and dipeptide-based chain extenders for soft tissue engineering. *J. Biomater. Sci. Polym. E* **2010**, *21*, 843–862. [CrossRef] [PubMed]
8. Manzoor, A.; Bin, X.; Purnawali, H.; Fu, Y. High performance shape memory polyurethane synthesized with high molecular weight polyol as the soft segment. *J. Appl. Sci.* **2012**, *2*, 535–548.
9. Oprea, S. Structure and properties of cross-linked polyurethane copolymers. *J. Adv. Polym. Technol.* **2009**, *28*, 165–172. [CrossRef]
10. Bai, H.C.; Tao, L.; Pang, Y.J.; Zhou, Y.J. Synthesis and characterization of hydroxypropyl terminated polydimethylsiloxane-polyurethane copolymers. *J. Appl. Polym. Sci.* **2013**, *129*, 2152–2160. [CrossRef]
11. Li, C.; Yu, X.; Speckhard, T.A.; Cooper, S.L. Synthesis and properties of polycyanoethylmethylsiloxane polyurea urethane elastomers: A study of segmental compatibility. *J. Polym. Sci. Pol. Phys.* **1988**, *26*, 315–337. [CrossRef]
12. Marcos-Fernandez, A.; Lozano, A.E.; González, L.; Rodríguez, A. Hydrogen bonding in copoly (ether-urea)s and its relationship with the physical properties. *J. Macromol.* **1997**, *30*, 3584–3592. [CrossRef]
13. Špírková, M.; Pavličević, J.; Strachotaa, A.; Porebaa, R. Novel polycarbonate-based polyurethane elastomers: Composition–property relationship. *J. Eur. Polym. J.* **2011**, *47*, 959–972. [CrossRef]
14. Adhikari, R.; Gunatillake, P.A.; McCarthy, S.J.; Bown, M. Low-modulus siloxane–polyurethanes. Part II. Effect of chain extender structure on properties and morphology. *J. Appl. Polym. Sci.* **2003**, *87*, 1092–1100. [CrossRef]
15. Shokrolahi, F.; Yeganeh, H. Soft segment composition and its influence on phase-separated morphology of PCL/PEG-based poly (urethane urea)s. *J. Iran. Polym. J.* **2014**, *23*, 505–512. [CrossRef]
16. Fragiadakis, D.; Runt, J. Molecular dynamics of segmented polyurethane copolymers: Influence of soft segment composition. *J. Macromol.* **2013**, *46*, 4184–4190. [CrossRef]
17. Mingjie, H.; Wei, F.; Le, G.; Weibing, W. One-pot synthesis of hyperbranched polyols and their effects as crosslinkers on HTPB-based polyurethane. *J. Polym. Bull.* **2014**, *71*, 2671–2693. [CrossRef]
18. Król, P.; Pielichowska, K.; Byczyńskia, Ł. Thermal degradation kinetics of polyurethane–siloxane anionomers. *J. Thermochim. Acta* **2010**, *507*, 91–98. [CrossRef]
19. Castagna, A.M.; Fragiadakis, D.; Lee, H.; Choi, T. The role of hard segment content on the molecular dynamics of poly (tetramethylene oxide)-based polyurethane copolymers. *J. Macromol.* **2011**, *44*, 7831–7836. [CrossRef]
20. Wang, D.; Zhang, G.; Zhang, Y.; Gao, Y. Synthesis, characterization, and properties of novel polyetherester polyols and developed polyurethanes. *J. Appl. Polym. Sci.* **2007**, *103*, 417–424. [CrossRef]
21. Chattopadhyay, D.K.; Raju, K. Structural engineering of polyurethane coatings for high performance applications. *J. Prog. Polym. Sci.* **2007**, *32*, 352–418. [CrossRef]

22. Fu, H.; Gao, H.; Wu, G.; Wang, Y. Preparation and tunable temperature sensitivity of biodegradable polyurethane nanoassemblies from diisocyanate and poly (ethylene glycol). *J. Soft Matter* **2011**, *7*, 3546–3552. [CrossRef]
23. Mondal, S.; Martin, D. Hydrolytic degradation of segmented polyurethane copolymers for biomedical applications. *J. Polym. Degrad. Stab.* **2012**, *97*, 1553–1561. [CrossRef]
24. Oprea, S. Degradation of crosslinked poly (ester-urethanes) elastomers in distilled water: Influence of hard segment. *J. Appl. Polym. Sci.* **2012**, *124*, 1059–1066. [CrossRef]
25. Salacinski, H.J.; Odlyha, M.; Hamilton, G.; Seifalian, A.M. Thermo-mechanical analysis of a compliant poly (carbonate-urea) urethane after exposure to hydrolytic, oxidative, peroxidative and biological solutions. *J. Biomater.* **2002**, *23*, 2231–2240. [CrossRef]
26. Kultys, A.; Rogulska, M.; Pikus, S.; Skrzypiec, K. The synthesis and characterization of new thermoplastic poly (carbonate-urethane) elastomers derived from HDI and aliphatic–aromatic chain extenders. *J. Eur. Polym. J.* **2009**, *45*, 2629–2643. [CrossRef]
27. Seifalian, A.M.; Salacinski, H.J.; Tiwan, A.; Edwards, A. In vivo biostability of a poly (carbonate-urea) urethane graft. *J. Biomater.* **2003**, *24*, 2549–2557. [CrossRef]
28. Pergal, M.V.; Antić, V.V.; Govedarica, M.N.; Goäevac, D. Synthesis and characterization of novel urethane-siloxane copolymers with a high content of PCL-PDMS-PCL segments. *J. Appl. Polym. Sci.* **2011**, *122*, 2715–2730. [CrossRef]
29. Zhu, R.; Wang, Y.; Zhang, Z.; Ma, D. Synthesis of polycarbonate urethane elastomers and effects of the chemical structures on their thermal, mechanical and biocompatibility properties. *J. Heliyon* **2016**, *2*, e00125. [CrossRef] [PubMed]
30. Wang, Y.; Wang, X.; Shi, J.; Zhu, R. Flexible silk fibroin films modified by genipin and glycerol. *J. RSC Adv.* **2015**, *5*, 101362–101369. [CrossRef]
31. Choi, T.; Masser, K.A.; Moore, E.; Weksler, J. Segmented polyurethanes derived from novel siloxane–carbonate soft segments for biomedical applications. *J. Polym. Sci. Pol. Phys.* **2011**, *49*, 865–872. [CrossRef]
32. Wang, C.B.; Cooper, S.L. Morphology and properties of segmented polyether polyurethaneureas. *J. Macromol.* **1983**, *16*, 775–786. [CrossRef]
33. Oprea, S.; Potolinca, V.O.; Oprea, V. Synthesis and properties of new crosslinked polyurethane elastomers based on isosorbide. *J. Eur. Polym. J.* **2016**, *83*, 161–172. [CrossRef]
34. Cassie, A.B.D.; Baxter, S. Wettability of porous surfaces. *J. Trans. Faraday Soc.* **1944**, *40*, 546–551. [CrossRef]
35. Seo, J.H.; Kakinoki, S.; Inoue, Y.; Nam, K. The significance of hydrated surface molecular mobility in the control of the morphology of adhering fibroblasts. *J. Biomater.* **2013**, *34*, 3206–3214. [CrossRef] [PubMed]
36. Extrand, C.W.; Kumagai, Y. An experimental study of contact angle hysteresis. *J. Colloid Interface Sci.* **1997**, *191*, 378–383. [CrossRef] [PubMed]
37. Sheikhy, H.; Shahidzadeh, M.; Ramezanzadeh, B.; Noroze, F. Studying the effects of chain extenders chemical structures on the adhesion and mechanical properties of a polyurethane adhesive. *J. Ind. Eng. Chem.* **2013**, *19*, 1949–1955. [CrossRef]
38. Jiang, S.; Ji, X.; An, L.; Jiang, B. Crystallization behavior of PCL in hybrid confined environment. *J. Polym.* **2001**, *42*, 3901–3907. [CrossRef]
39. De Groot, J.H.; De Vrijer, R.; Wildeboer, B.S.; Spaans, C.S. New biomedical polyurethane ureas with high tear strengths. *J. Polym. Bull.* **1997**, *38*, 211–218. [CrossRef]
40. Miller, J.A.; Lin, S.B.; Hwang, K.K.S.; Wu, K.S.; Gibson, P.E.; Cooper, S.L. Properties of polyether-polyurethane block copolymers: Effects of hard segment length distribution. *J. Macromol.* **1985**, *18*, 32–44. [CrossRef]
41. Eceiza, A.; Martin, M.D.; De la Caba, K.; Kortaberria, G. Thermoplastic polyurethane elastomers based on polycarbonate diols with different soft segment molecular weight and chemical structure: Mechanical and thermal properties. *J. Polym. Eng. Sci.* **2008**, *48*, 297–306. [CrossRef]
42. Teramoto, N.; Saitoh, Y.; Takahashi, A.; Shibata, M. Biodegradable polyurethane elastomers prepared from isocyanate-terminated poly(ethylene adipate), castor oil, and glycerol. *J. Appl. Polym. Sci.* **2010**, *115*, 3199–3204. [CrossRef]
43. Chiou, B.S.; Schoen, P.E. Effects of crosslinking on thermal and mechanical properties of polyurethanes. *J. Appl. Polym. Sci.* **2002**, *83*, 212–223. [CrossRef]

44. Shi, H.; Lan, T.; Pinnavaia, T.J. Interfacial effects on the reinforcement properties of polymer-organoclay nanocomposites. *J. Chem. Mater.* **1996**, *8*, 1584–1587. [CrossRef]
45. Rueda-Larraz, L.; d'Arlas, B.F.; Tercjak, A.; Ribes, A. Synthesis and microstructure–mechanical property relationships of segmented polyurethanes based on a PCL–PTHF–PCL block copolymer as soft segment. *J. Eur. Polym. J.* **2009**, *45*, 2096–2109. [CrossRef]
46. Wen, X.W.; Pei, S.P.; Li, H.; Ai, F. Study on an antifouling and blood compatible poly (ethylene–vinyl acetate) material with fluorinated surface structure. *J. Mater. Sci.* **2010**, *45*, 2788–2797. [CrossRef]
47. Balakrishnan, B.; Banerjee, R. Biopolymer-based hydrogels for cartilage tissue engineering. *J. Chem. Rev.* **2011**, *111*, 4453–4474. [CrossRef] [PubMed]
48. Han, W.; Tu, M.; Zeng, R.; Zhao, J. Preparation, characterization and cytocompatibility of polyurethane/cellulose based liquid crystal composite membranes. *J. Carbohyd. Polym.* **2012**, *90*, 1353–1361. [CrossRef] [PubMed]
49. ASTM F 756-00. *Standard Practice for Assessment of Hemolytic Properties of Materials*; American Society for Testing and Materials: Philadelphia, PA, USA, 2000.
50. Lönnroth, E.C.; Dahl, J.E. Cytotoxicity of liquids and powders of chemically different dental materials evaluated using dimethylthiazol diphenyltetrazolium and neutral red tests. *J. Acta Odontol. Scand.* **2003**, *61*, 52–56. [CrossRef]
51. Barrioni, B.R.; de Carvalho, S.M.; Oréfice, R.L.; de Oliveira, A.A.R. Synthesis and characterization of biodegradable polyurethane films based on HDI with hydrolyzable crosslinked bonds and a homogeneous structure for biomedical applications. *J. Mater. Sci. Eng. C* **2015**, *52*, 22–30. [CrossRef] [PubMed]
52. Lönnroth, E.C. Toxicity of medical glove materials: A pilot study. *Int. J. Occup. Saf. Ergon.* **2005**, *11*, 131–139. [CrossRef] [PubMed]
53. De Oliveira, A.A.R.; de Carvalho, S.M.; Leite, M.D.F.; Oréfice, R.L. Development of biodegradable polyurethane and bioactive glass nanoparticles scaffolds for bone tissue engineering applications. *J. Biomed. Mater. Res. B Appl. Biomater.* **2012**, *100*, 1387–1396. [CrossRef] [PubMed]